J. Appl. Comput. Mech., xx(x) (2026) 1-15
DOI: 10.22055/jacm.2026.48653.5397

ISSN: 2383-4536
jacm.scu.ac.ir

Shahid Chamran
University of Ahvaz

Journal of
Applied and Computational Mechanics

Research Paper

Modeling Complex Flow and Heat Transfer in Engine Oil Suspended with Gr/MgO/Cu Nanoparticles Using Fractal-Fractional Derivatives

Gohar Ali[1], Dolat Khan[2], Zeeshan Ali[3]

[1] Department of Mathematics, City University of Science & Information Technology, Peshawar, KPK, Pakistan, Email: goharali.cu@gmail.com

[2] Department of Mathematics, Saveetha School of Engineering, SIMATS, Chennai, Tamil Nadu, India, Email: dolat.ddk@gmail.com

[3] Department of Information Management, National Yunlin University of Science and Technology: Douliu, Yunlin, Taiwan, Email: zeeshan@yuntech.edu.tw

Received July 30 2025; Revised March 25 2026; Accepted for publication April 25 2026.
✉ Corresponding author: G. Ali (goharali.cu@gmail.com)

Abstract. Industrial applications of diathermal oils have sparked significant interest in recent years, driving innovation in thermal management. This study revolutionizes the field by developing a new fractal-fractional model for analyzing the thermal enactment of three nanoparticles (graphene, magnesium oxide, copper nanoparticles) in channel flows. We create a robust industrial fluid by homogeneously dispersing the dust particles in engine oil. Model the separate momentum equations for the engine oil base fluid velocity and dust particle velocity profiles, yielding exact solutions for both velocity profiles and temperature profiles. The mentioned physical phenomena are expressed through a mathematical model using a fractal fractional derivative based on a power law kernel. The problem has been solved using classical and fractal Laplace transform methods. On solving these problems, it has been possible to calculate the heat transfer rates, shear stresses, and skin friction coefficients. This research work shows a 9.98% improvement in the heat transfer coefficient of engine oil, which proves it to be a good lubricant. Fractal fractional derivatives give a clear insight into memory effects. The proposed model surpasses traditional models based on fractional derivatives, offering improved results. The valuable aspect of this research study lies in its applicability to give a paradigm shift to industries. It will be helpful in designing efficient thermal management systems. The proposed fractal fractional model has a clear edge in terms of memory effect performance. It has been applicable in modeling complicated dynamics of fluids. It could be used for hydraulic fracturing processes. The improved lubrication system for mechanical, advanced cooling system for electronics, and advanced thermal management for aeronautical engineering are applications of this study. The temperature distribution graph peaks for the Eo-MgO-Cu-Gr nanofluid, surpassing the graphs of all other examined combinations.

Keywords: Dust particles, Shape effects, Tri-hybrid nanoparticles, Fractal fractional model, Base fluid engine oil.

1. Introduction

The Riemann-Liouville fractional calculus often uses the Riemann-Liouville derivative [1], which has been and remains one of the most universally accepted definitions of non-integer order derivations. Nonetheless, its most important disadvantage is its inability to vanish on constant functions. To resolve this problem, Caputo proposed a new definition of the fractional derivative known today as the Caputo derivative [2]. Nonetheless, all of these new developments are still plagued with singular kernels. To resolve this problem and capitalize on previous developments on fractional calculus, Caputo and Fabrizio proposed another new model of fractional calculus with a non-singular kernel [3]. This new model provided another sophisticated means of studying fractional processes. Currently, all of these have generated considerable interests among many persons who are searching and investigating various definitions of fractional derivatives and their uses in many branches of science [4-6]. Several studies have explored the use of Caputo and Fabrizio time-fractional derivatives in modeling various physical phenomena. Despite offering improvements over earlier models, the Caputo-Fabrizio approach still suffers from the limitation of having a local kernel, which restricts its ability to fully capture memory and spatial effects in complex systems. To address this limitation, a new fractional-order operator was introduced by researchers who incorporated the Mittag-Leffler function into the kernel structure. This advancement resulted in derivatives that are both nonlocal and nonsingular, enhancing their suitability for modeling real-world processes. These new fractional derivatives were later applied to analyze a simple nonlinear system, where both the existence and uniqueness of solutions were rigorously studied. Further research, based on this foundation, extended the application of this derivative model in probing the dynamic behavior of Chua's circuit and demonstrated its usefulness in chaotic and electrical studies [7-9]. In recent times, the scientific researchers have been increasingly applying improved fractional derivative methods to

Published online: April 27 2026

deal with difficult mathematical models involving variable and complex orders. These methods have been found to be quite effective in the investigation of problems related to fluid dynamics, heat conduction, and mass transport. One of the newer developments involves the fractal-fractional derivative method. However, this has not yet been applied to problems of the order of heat transfer in channel flows. To fill this lacuna, a new method was proposed which consisted of the application of a fractal-fractional derivative of variable order with a power-law kernel for modeling natural convection heat transfer between two stationary vertical plates by Khan et al. [10]. Subsequent studies have also shown that the combination of fractional derivatives with nonlocality and memory and fractal properties is required to provide more accurate representations of the complex physical systems which traditional and classical fractional models are usually unable to depict by Turkyilmazoglu and Alofi [11]. Furthermore, Hilfer-type fractal-fractional derivative as given by Shloof et al., [12], along with operational matrix methods, has also been applied with success in solving differential equations obtained in such contexts. Another novel application was presented for heat transfer analysis in a vertical channel, wetted by a nanofluid made with water and clay-based nanoparticles. In this study, fractal-fractional derivative of variable order in time with a power-law kernel was applied to investigate the problem of thermal transfer caused especially by the flow of the fluid between two fixed vertical plates, one of whose walls continuously heated. Such developments indicate that fractal-fractional calculus will play an increasingly vital role and will find wider applications in solving intricate engineering and physical problems [13].

The phenomenon of flow and heat transfer in nanofluids and particularly intricate tri-hybrid nanofluids with suspended dust particles has certain physical processes that standard and fractional modeling is unable to reproduce. The processes involve are, the mixing of nanoparticles and dust particles leads to a non-standard diffusion process. The diffusion process of heat and momentum is no longer standard and relies on Fick's laws. Heat and momentum diffuse via a power-law distribution pattern. This corresponds to fractional dynamics with power-law kernels. The state of the fluid is dependent upon its past evolution in terms of its thermodynamics. The interaction and collision between dust particles and nanoparticles and also between nanoparticles and the fluid do not happen instantaneously. The phenomenon has long-term effects. The effects of interaction and collision between all types of matter involved do not vanish instantaneously. The phenomenon can be described with help of fractional calculus. The nanoparticles tend to form clusters. The path of suspended dust particles also behaves like fractals. A fractal object has self-similarity. The object seems similar at all sizes and from all angles. The structure and topology of fractals can't be defined with standard calculus. Fractal calculus is required. A fractal model of nanofluids can therefore accommodate both fractal geometry and memory effects. The fractal and fractional model of nanofluids can therefore be termed physical.

In today’s modern and technological era, there is more focus on developing materials that are not only highly efficient and functional but also compact in size, which is required for products like smartphones and laptops. This technological requirement has opened doors to progress in nanotechnology, an area of science that is rapidly growing. Nanotechnology deals with material engineering based on a nanometric scale or even a supramolecular scale, through state-of-the-art technology of production. The advantages that nanotechnology provides a number of benefits such as cost-reducing in production, greater efficiency of resource utilization, better quality of material, and improvement in the standard of living. The scientific potential of nanotechnology provides an opportunity for scientists. vast, resulting in inventions of new devices in different fields such as consumer electronics, medical science, automobile manufacturing, and renewable energy resources. nanotechnology has immense importance in solving heat transfer problems with the help of nanofluids. These engineered fluids are designed to enhance thermal properties, meeting the demands of various industrial systems that require efficient heat dissipation. In conventional fluids, there often exist limitations regarding thermal characteristics. In such cases, innovative methods have been developed to enhance thermal performance. The invention of nanofluids has radically changed this sector by enhancing heat transfer rates, resistance to corrosion, and anti-wear characteristics. Recent years have seen extensive explorations regarding different aspects of nanofluid flow and heat transfer. Various aspects of nanofluid flow and heat transfer have been explored recently. A profound exploration of nanofluid flow dynamics and accompanying heat transfer processes have been carried out by Gangadhar et al. [14]. The work includes different complex processes. The scope includes hybrid nanofluids. Experiments were conducted on wall jet plasma flow with consideration for Joule heating. Another scope includes exploration of Carreau fluid with triple nanoparticles. The scope is associated with the stretched surface. The exploration includes particular attention to ohmic dissipation. The scope further includes explorations regarding Maxwell fluid flow. The fluid flow includes homogeneous and heterogeneous chemical reactions. The exploration includes rotation disks. The exploration is associated with numerical and machine learning approach-based evaluations. Another scope includes exploration of Oldroyd-B nanofluid flow. The flow is associated with triple-layered porous mediums. The exploration is associated with bioconvection caused by gyrotactic microorganisms. The scope also includes particular attention to nonlinear thermal radiation. The explorations were carried out as reported in [15-17]. Complementing these efforts, other researchers have adopted numerical methods such as the Crank-Nicolson scheme to explore thermal performance enhancements in three-dimensional convective flow of Walter-B fluids with nanoparticle suspensions around cylindrical geometries investigated by Wang et al., [18]. Additional, Kotha et al. [19] studies have also considered the influence of internal heat generation in magnetohydrodynamic nanofluid flows, driven by the motion of gyrotactic microorganisms, to understand bioconvective transport behavior in such systems. Research on nanofluids, including thermal transport in radioactive fluids with microorganisms, has deepened understanding of advanced heat transfer. Oil-based and particle-laden (dusty) nanofluids show improved thermal and mechanical efficiency, making them valuable for modern industrial uses by Gangadhar et al., [20]. Graphene-based nanofluids have been found to enhance the efficiency of polymerase chain reactions, and their tunable optical properties make them promising candidates for solar energy collectors, as demonstrated in recent studies [21-23]. Tian et al., [24] examined the thermal conductivity properties of a hybrid nanofluid composed of graphene oxide and Al_2O_3 suspended in a water-ethylene glycol mixture. Contrary to these studies, Alkasmoul et al., [25] reviewed the utilization of nanofluids in solar collectors but overlooked the influence of Brownian motion in improving heat transfer. In another study, Khan et al., [26] examined the application of a fractional order model in drilling processes, establishing the efficacy of hybrid nanofluids with internal heating. Development in nanotechnology has culminated in emerging hybrid nanostructures, so-called hybrid nanofluids, which attract immense attention in the scientific community. Indeed, various research works on hybrid nanofluids emphasizing advances in this emerging technology were done by Leong et al. [27]. In fluid dynamics, Khan et al. [28] performed an analytical study on the transient Magnetohydrodynamics (MHD) flow in a rotating frame of a hybrid second-grade fluid nano-fluid using the Laplace and Sumudu transforms in determining fluid flow behavior. Similarly, in heat transfer studies on hybrid nano-fluids, Saqib et al., [29] used integral transforms for solving fractional differential equations for heat transfer analysis in hybrid nano-fluids. In emphasizing developments in utilizing sun energy, Esmaeili et al., [30] discussed an enhancement in heat transfer in Parabolic Trough Solar Collectors (PTCs) using a hybrid arrangement of turbulators and nanofluids for improving efficiency in PTCs. In another aspect concerning heat transfer in hybrid nano-fluids, an analysis on entropy generation with thermal characteristics of a hybrid nano-fluid flow with a Williamson model with application in a Solar Aircraft using a Parabolic Trough Solar Collector for cooling purposes for energy production in an SCA with a PTC by Hussain [31]. In the automotive sector, Esfe et al. [32] employed artificial neural networks to predict the thermal conductivity of hybrid nanofluids, aiming to enhance engine oil efficiency. He et al. [33] studied electromagnetic nanofluid flow, revealing complex interactions between nanoparticles, temperature, and viscosity, which are crucial for thermal management system design. Additionally, He and Abd Elazem [33] developed a carbon nanotube-embedded boundary layer theory, unlocking new possibilities for efficient energy harvesting and conversion.

Those fluids that obey the viscous and as well as elastic properties are known as Brinkman-type fluids. The characteristics of Brinkman-type fluid are, the resistance to shear stress, like traditional fluids this is a viscosity characteristic. And if the fluid can store the energy and return to its original shape, like solids, this is an elasticity characteristic. The Brinkman-type fluids are the generalization of Navier Stokes fluids. These fluids are used in, Polymer solutions, Blood flow models, Viscoelastic fluids models, and Fluid-structure interactions. These fluids were first introduced by Brinkman in 1949 [35]. Khan et al., [36] studied the hydromagnetic Brinkman-type fluid in a permeable porous medium with Darcy medium and the effect of heat transfer. In this investigation, the authors analyze the main objectives of stress and heat transfer rate on velocity profile on Brinkman fluid and temperature profile. In another, research by Khan et al., [37] the Brinkman fluid between two side walls bovver an infinite parallel plate according to Stokes problem for transient flow. This study has a wide range of applications in the real world, like biological fluid dynamics, chemical engineering, geophysical fluid dynamics, materials science, and microfluidics. The effects of MHD-free convectional flow, heat transfer, and variable temperature on generalized dusty Brinkman-type fluid with significant consequences for real-world applications, including electrochemical engineering, aerospace engineering, environmental engineering, and biotechnology was reported by Khan et al., [38]. Also, this model (the generalized model) can help other research societies and engineers, like more efficient heat transfer systems designed, for environmental remediation to develop new technologies, and most importantly for drug delivery systems.

The solid particles or dust particles distributed in fluid flow are known as dusty fluid flow [39-40]. Dusty fluid flow is a type of multiphase flow. New multiphase flows are used physically. Also, the dusty phase flow is known as a two-phase flow. The application of dusty fluid flow in various fields, including aerospace engineering, chemical engineering, and environmental engineering. Understanding dusty fluid flow is crucial for, predicting particle transport and deposition, Modeling pollutant dispersion, and Designing filtration systems. Khan et al., [41] investigated the Couette flow of dusty fluid in the rotating frame, with Newtonian heating and heat transfer. This study provides valuable insights into the thermodynamic efficiency and irreversibility of the process, helping researchers and engineers, develop more efficient thermal energy storage systems, and improve bioreactor design and performance. Rostami et al., [42] investigated the predict the thermal conductivity of SiO_2/water–ethylene glycol (50:50) hybrid nanofluid using artificial neural network particles. Nowadays, many researchers study dusty fluids in different fields of fluid dynamics [43].

Each of these nanoparticles – graphene, copper, and magnesia – displays distinct characteristics that enable them to find practical applications. For instance, magnesia (MgO) nano-particles offer high physical and chemical strength, high thermal conductivity, and are used for construction, medical applications, and optical technology. Another nano-particle is graphene. In this case, graphene exhibits high strength and transparency. It can find practical uses for applications involving electronic devices, energy storage, and biological engineering. Electrical and high thermal conductivity render copper nano-particles useful for uses such as electrical wiring and plumbing. The present work focuses on examining the effect of such nano-particles on heat flow, perceiving their substantial physical characteristics and uses.

Zuo fractal ridge theory [44] on nano/micro fluid lubrication based on fractal surface topography for shaft and bearing contact describes fractal rheological model equations using both fractal concept and equations for better tribological insight. Kou et al.'s [45] critical assessment of basic fractal boundary layers helps to better understand our work. An excellent work in fluid dynamics domain to date is to cultivate fractal fractional derivatives for mathematical models. This fusion of ideas helps to better understand complex phenomena with ease. The fractional model is very good to interpret real-world phenomena. The fractal model is very effective to interpret complexities. The fusion of fractal and fractional models helps to exactly interpret fluid dynamics. In fact, fractal fractional models can appropriately model parameters to match experimental data and mathematical expressions exactly. The fractal fractional model is very helpful to interpret crossover phenomena. The fusion of fractal and fractional models helps to clearly understand viscoelastic fluid dynamics. They can exactly interpret fluid dynamics phenomena. The fractal fractional model is helpful to model any fluid dynamics scenario at different time frames. The fractal fractional model is very helpful to clearly understand viscoelastic fluid dynamics phenomena. They can exactly interpret fluid dynamics. The fractal fractional model is helpful to clearly interpret viscoelastic fluid dynamics. They can exactly interpret fluid dynamics phenomena. The fractal fractional model can exactly interpret fluid dynamics phenomena. The fractal fractional model can exactly interpret fluid dynamics. The fractal fractional model can exactly interpret viscoelastic fluid dynamics. They can exactly interpret fluid dynamics. The fractal fractional model can exactly interpret fluid dynamics. The fractal fractional model can exactly interpret fluid dynamics phenomena. The fractal fractional model can exactly interpret viscoelastic fluid dynamics phenomena. They can exactly interpret fluid dynamics. The fractal fractional model can exactly interpret fluid dynamics. The fractal fractional model can exactly interpret viscoelastic fluid dynamics.

As per our information, a research study has not been conducted on an oil-based tripartite hybrid nanoparticle using a dusty Brinkman-type fluid at a unidirectional, one-dimensional, unsteady flow. With the use of fractal fractional modeling, we are able to expose both nanofluids' thermal behaviors and characteristics. This has never been done before:

- It introduces a separate momentum equation for oil-based Brinkman-type fluid and a dusty fluid.
- Also, the dust particles are evenly dispersed in the oil fluid.
- We derive a fractal-fractional approach to investigate tripartite hybrid nanofluids, which is introduced to the scientific literature.
- We give exact solutions for this model, and this is quite uncommon in the literature.
- Our study covers different shapes for the nanoparticles, thereby making our results more meaningful.

This extensive research work is an excellent opportunity for us to present an in-depth assessment of bi-tri hybrid nanofluids. The work is expected to shed light on energy distribution and characteristics, flow behaviors, parameters, skin friction, and heat transfer capabilities. This innovative work is expected to help us unlock and unleash the full potential of bi-tri hybrid nanofluids for practical uses such as improvement of lubrication and heat transfer processes.

1.1. Limitations and potential scalability of nanofluid

This study employs established theoretical models and mixing rules to estimate the thermophysical properties of the tri-hybrid nanofluid. It is important to acknowledge that these models may not fully capture the complex interactions (e.g., aggregation, synergistic effects) between the different nanoparticles (Gr, MgO, Cu). These interactions could influence the effective viscosity and thermal conductivity, potentially leading to deviations between the theoretical predictions and experimental data. Future work will involve experimental validation to refine these models for multi-hybrid nanofluids. Despite the enhanced thermal performance predicted in this study, the proposed nanofluid is subject to several limitations. The analysis assumes uniform nanoparticle dispersion and constant thermophysical properties, which may not fully represent industrial operating conditions.

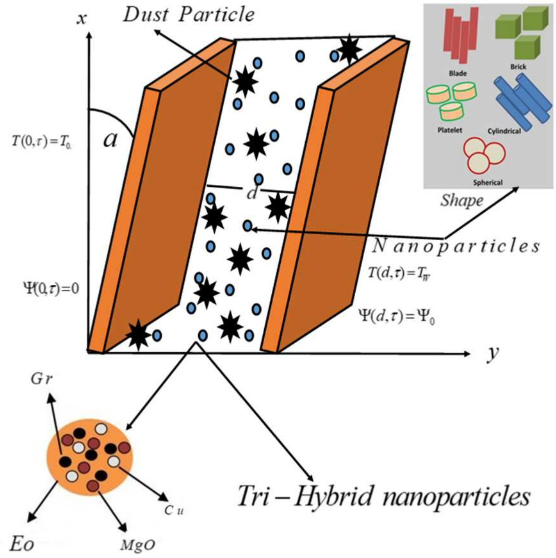

Fig. 1. The geometry of the given flow Model.

Practical challenges such as nanoparticle agglomeration, stability issues, increased viscosity, and higher pumping power requirements may affect large-scale performance. Furthermore, considerations related to cost, long-term reliability, and industrial scalability require further experimental validation before practical implementation.

2. Problem Statement

The following assumptions are for the present flow regime:

- The present study assumes a laminar, unidirectional, one-dimensional, and unsteady flow regime, with engine oil as the base fluid.
- The dusty particles are considered throughout the basic fluid distributed homogeneously.
- Trihybrid nanoparticles (*Gr, MgO, Cu*) are suspended between two infinite parallel plates, forming a vertical channel geometry with a length d (Fig. 1) [33-34].
- Initially, the plates and fluid are stationary, with radiation effects introduced from the left end.
- The channel plates are varied from T_0, and T_W, the heat transfer process takes place.
- The right plate moves with constant velocity like, Ψ_0, then the fluid flows.
- Thermal equilibrium is established between the nanoparticles and the host fluid.
- Radiative flux in the parallel direction is negligible compared to the perpendicular direction.
- Pressure gradient effects are insignificant in this process.
- Also take the inclination in both plates, i.e $\cos(a)$.

The following mathematical equations governing the energy and flow fields are obtained by invoking the Rosseland and Boussinesq approximations [46-50]:

$$\left.\begin{aligned} &\nabla.\vec{V}(y,\tau)=0,\\ &\vec{V}(y,\tau)=\Psi(y,\tau)\hat{i}\\ &\vec{V}_1(y,\tau)=\Psi_1(y,\tau)\hat{i}\\ &T(y,\tau)=T(y,\tau)\end{aligned}\right\} \tag{1a}$$

$$\left[\frac{\partial\Psi(y,\tau)}{\partial\tau}+\beta_1\Psi(y,\tau)\right]=\frac{\mu_{thnf}}{\rho_{thnf}}\frac{\partial^2\Psi(y,\tau)}{\partial y^2}+g\frac{(\rho\beta)_{thnf}}{\rho_{thnf}}\{T(y,\tau)-T_0\}\cos(a)-K_0N_0\left(\Psi(y,\tau)-\Psi_1(y,\tau)\right), \tag{1b}$$

$$\frac{\partial T(y,\tau)}{\partial\tau}=\left(\frac{K}{(\rho C_p)}\right)_{thnf}\left[1+\frac{16\sigma_0T_0^3}{(3\kappa_0)K_{thnf}}\right]\frac{\partial^2T(y,\tau)}{\partial y^2}. \tag{2}$$

The ICs, and BCs are:

$$\left.\begin{aligned} &\Psi(y,0)=\Psi_1(y,0)=0, T(y,0)=T_{0.} \quad y>0\\ &\Psi(0,\tau)=0, T(0,\tau)=T_{0.} \quad \tau>0\\ &\Psi(d,\tau)=\Psi_0, T(d,\tau)=T_W\end{aligned}\right\} \tag{3}$$

The momentum equation for dust particle is:

$$\frac{\partial\Psi_1(y,\tau)}{\partial\tau}=\frac{K_0}{m}\left(\Psi(y,\tau)-\Psi_1(y,\tau)\right), \tag{4}$$

Table 1. The viscosity of different nanoparticles.

Blade shape *Gr* nanoparticles	$\mu_{nf,1} = \mu_{EO}\left(14.6\Omega_{Gr} + 123.3\Omega_{Gr}^2 + 1\right)$
Platelet shape *MgO* nanoparticles	$\mu_{nf,2} = \mu_{EO}\left(37.1\Omega_{Mgo} + 612.6\Omega_{Mgo}^2 + 1\right)$
Sphere shape *Cu* nanoparticles	$\mu_{nf,3} = \mu_{EO}\left(2.5\Omega_{Cu} + 6.2\Omega_{Cu}^2 + 1\right)$

Table 2. The specific heat capacity and thermal expansion coefficient of a nanofluid.

Name of nanofluid	Specific heat capacity	Thermal expansion coefficient
Nanofluid	$(\rho C_p)_{nf} = (\rho C_p)_{hf} - \Omega_{np}\left\{(\rho C_p)_{hf} - (\rho C_p)_{np}\right\}$	$(\rho\beta_p)_{nf} = (\rho\beta_p)_{hf} - \Omega_{np}\left\{(\rho\beta_p)_{hf} - (\rho\beta_p)_{np}\right\}$
Tripartite hybrid nanofluid	$(\rho C_p)_{thnf} = (1-\Omega_{Gr}-\Omega_{Mgo}-\Omega_{Cu})(\rho C_p)_{Eo} + \Omega_{Gr}(\rho C_p)_{Gr} + \Omega_{Mgo}(\rho C_p)_{Mgo} + \Omega_{Cu}(\rho C_p)_{Cu}$	$(\rho\beta)_{thnf} = (1-\Omega_{Gr}-\Omega_{Mgo}-\Omega_{Cu})(\rho\beta)_{Eo} + \Omega_{Gr}(\rho\beta)_{Gr} + \Omega_{Mgo}(\rho\beta)_{Mgo} + \Omega_{Cu}(\rho\beta)_{Cu}$

Table 3. The density of the base fluid and the dispersed nanoparticles.

Name particles	Density
Nanoparticle	$\rho_{nf} = \Omega_{np}\rho_{np} + \rho_{hf} - \Omega_{np}\rho_{hf}$
Tripartite hybrid nanoparticle	$\rho_{thnf} = (1-\Omega_{Gr}-\Omega_{Mgo}-\Omega_{Cu})\rho_{Eo} + \Omega_{Gr}(\rho_{Gr}) + \Omega_{Mgo}(\rho_{Mgo}) + \Omega_{Cu}(\rho_{Cu})$

Table 4. Computational values for *a*, *b*, and *m* [55].

Shapes	*a*	*b*	*m*
Blade	14.6	123.3	8.3
Cylinder	13.5	909.4	4.9
platelet	37.1	612.6	5.7
Brick	1.9	471.4	3.7
Spherical	2.5	6.2	3.0

Table 5. The thermal conductivity of different nanoparticles.

Name or shape of nanoparticles	Thermal conductivity
General	$\dfrac{K_{nf}}{K_{nf}} = \dfrac{(m-1)K_{hf}(m-1) + K_{np} - (m-1)\left(K_{hf} - K_{np}\right)\Omega_{np}}{K_{hf}(m-1) + K_{np} - \left(K_{hf} - K_{np}\right)\Omega_{np}}$
Blade shape Gr nanoparticles	$\dfrac{K_{nf,1}}{K_{Eo}} = \dfrac{7.3K_{Eo} + K_{Gr} - 7.3\Omega_{Gr}(K_{Eo} - K_{Gr})}{7.3K_{Eo} + K_{Gr} - \Omega_{Gr}(K_{Gr} - K_{Eo})}$
Platelet shape MgO nanoparticles	$\dfrac{K_{nf,2}}{K_{Eo}} = \dfrac{4.7K_{Eo} + K_{Mgo} - 4.7\Omega_{Mgo}\left(K_{Eo} - K_{Mgo}\right)}{4.7K_{Eo} + K_{Mgo} - \Omega_{Mgo}\left(K_{Mgo} - K_{Eo}\right)}$
Sphere shape Cu nanoparticles	$\dfrac{K_{nf,3}}{K_{Eo}} = \dfrac{2K_{Eo} + K_{cu} - 2\Omega_{cu}\left(K_{Eo} - K_{cu}\right)}{2K_{Eo} + K_{cu} - \Omega_{cu}\left(K_{cu} - K_{Eo}\right)}$
Combine of all three nanoparticles	$\Omega\left(K_{thnf}\right) = \Omega_{Gr}(K_{nf,1}) + \Omega_{MgO}(K_{nf,2}) + \Omega_{Cu}(K_{nf,3})$

3. Relations for Thermo-Physical Features

The following are the thermos-physical properties or features with their relations.

3.1. Viscosity

Table 1 shows boundary layer flow development is chiefly governed by viscous effects, drag forces, density, and thermal expansion. Furthermore, the flow patterns are notably impacted by the viscosity of nanofluids, which quantifies their resistance to deformation. To accurately determine the viscosity of a nanofluid, especially about nanoparticle shape, the following model should be employed [48]:

$$\mu_{nf} = \mu_{nf}\left(a\Omega_{np} + b\Omega_{np}^2 + 1\right), \tag{5}$$

where *a*, and *b* shows the specific shape of a nanoparticle, and Ω_{np} shows the volume concentration of particles is generally. The interpolation method enables the prediction of the viscosity of ternary hybrid nanofluids using the following relation [48]:

$$\Omega(\mu_{thnf}) = \Omega_{Gr}(\mu_{nf,1}) + \Omega_{Mgo}(\mu_{nf,2}) + \Omega_{Cu}(\mu_{nf,3}), \tag{6}$$

where $\Omega = \Omega_{Gr} + \Omega_{Mgo} + \Omega_{Cu}$, is net volume concentration.

3.2. Thermal expansion coefficient and specific heat capacitance

Table 2 shows the comprehensive analysis of the specific heat capacity and thermal expansion coefficient of nanofluids is presented in reference [49, 51-54], offering valuable insights into the thermal behavior and properties of nanofluids under different conditions, thereby deepening our understanding of their thermal dynamics.

3.3. Density

Table 3 presents formula used to describe the density of a nanofluid is presented in equation. This equation accounts for the combined density of the base fluid and the dispersed nanoparticles, providing a comprehensive understanding of the nanofluid's overall density. Table 4 shows the computational values of nanoparticle in the form its shapes.

3.4. Thermal conductivity

Table 5 investigated the thermal conductivity of nanoparticles is an important parameter that contributes to enhancing the heat conductibility of traditional fluids and is effective for better performance of advanced fluids in modern cooling industries. Coming up with accurate values of thermal conductivity is of prime value to set them effectively for nanofluids through calculations. Shape of nano-particles has good significance regarding thermal conductivity values, and you are required to integrate that factor into models related to calculations for effective results. Hamilton and Crosser's Model [56] assists in this context to provide effective thermal conductivity values by considering shapes of particles effectively and is helpful to prepare effective nanofluids.

4. Construction of Fractal-Fractional Model

There has been an explosion of innovation in new modeling approaches in recent years, and this has changed the paradigm in terms of understanding natural phenomena. A major development in this area is the incorporation of fractal and fractional derivatives in the traditional models, with all the approaches being integrated under one paradigm, allowing both derivatives to be applicable:

- Enhanced model accuracy, with results closely mirroring experimental data.
- Deeper insights into fluid rheology, capturing the memory effect with fractal and fractional operators.
- Flexible control over flow processes and thermal boundary layers, allowing for customized cooling rates.

Leveraging these advantages, this section develops a FFM by modifying Eqs. (1) to (4) using the power-law kernel. New factors are introduced to streamline the fundamental velocity and energy equations, defined as follows:

$$\tau^* = \frac{\upsilon \text{Eo}}{d^2}\tau,\quad \theta = \frac{T - T_0}{T_w - T_0},\quad \Psi^2 = \frac{\Psi}{\Psi_o}\ \beta_2 = \frac{\beta_1 d^2}{\upsilon \text{Eo}},\quad y^* = \frac{y}{d^2},\quad {\Psi_1}^2 = \frac{\Psi_1}{\Psi_{1o}}. \tag{7}$$

Apply Eq. (7) on Eqs. (1) to (4), we have:

$$f_1\left[\frac{\partial\Psi(y,\tau)}{\partial\tau} + \beta_2\Psi(y,\tau)\right] = f_2\frac{\partial^2\Psi(y,\tau)}{\partial y^2} + f_3 Gr_T\theta(y,\tau)\cos(a) - K\left(\Psi(y,\tau) - \Psi_1(y,\tau)\right), \tag{8}$$

$$\Pr\frac{\partial\theta(y,\tau)}{\partial\tau} = \left(\frac{f_5 + Nr}{f_4}\right)\frac{\partial^2\theta(y,\tau)}{\partial y^2}. \tag{9}$$

$$\left.\begin{array}{l} \Psi(y,0) = \Psi_1(y,0) = 0, \theta(y,0) = 0,\ y > 0 \\ \Psi(0,\tau) = 0, \theta(0,\tau) = 0,\quad \tau > 0 \\ \Psi(d,\tau) = 1,\qquad \theta(d,\tau) = 1 \end{array}\right\} \tag{10}$$

Using dimensionless variable to convert Eq. (4) in the following from:

$$\frac{\partial\Psi_1(y,\tau)}{\partial\tau} = \left(l_1\Psi(y,\tau) - l_2\Psi_1(y,\tau)\right), \tag{11a}$$

where,

$$\begin{gathered} l_1 = \frac{dK_0}{mw_0},\ l_2 = \frac{dK_0}{mw_{10}},\ Gr_T = \left(\frac{\beta_{Eo}}{\upsilon_{Eo}}\right)\frac{(T_w - T_0)gd^2}{\Psi_0},\quad Nr = \left(\frac{1}{K_{Eo}}\right)\frac{16\sigma_0 T_0^3}{3k_0},\ \Pr = \frac{(C_p\mu)_{Eo}}{K_{Eo}},\ K = \frac{K_0 N_0 d^2\Psi_0}{(\rho\upsilon)_{nf}\Psi_{10}}, \\ A_1 = \left(14.6\Omega_{Gr} + 123.3\Omega_{Gr}^2 - 1\right),\quad A_2 = \left(37.1\Omega_{MgO} + 612.6\Omega_{MgO}^2 - 1\right), \\ A_3 = \left(14.6\Omega_{Gr} + 123.3\Omega_{Gr}^2 - 1\right),\quad A_4 = \frac{7.3K_{Eo} + K_{Gr} - 7.3\Omega_{Gr}(K_{Eo} - K_{Gr})}{7.3K_{Eo} + K_{Gr} - \Omega_{Gr}(K_{Gr} - K_{Eo})}, \\ A_5 = \frac{4.7K_{Eo} + K_{Mgo} - 4.7\Omega_{Mgo}(K_{Eo} - K_{Mgo})}{4.7K_{Eo} + K_{MgO} - \Omega_{MgO}(K_{MgO} - K_{Eo})},\ A_6 = \frac{2K_{Eo} + K_{Cu} - 2\Omega_{Cu}(K_{Eo} - K_{Cu})}{2K_{Eo} + K_{Cu} - \Omega_{Cu}(K_{Cu} - K_{Eo})}, \\ f_1 = \left(1 - \Omega_{Gr} - \Omega_{MgO} - \Omega_{Cu}\right) + \left[\frac{\Omega_{Gr}(\rho_{Gr}) + \Omega_{MgO}(\rho_{MgO}) + \Omega_{Cu}(\rho_{Cu})}{\rho_{Eo}}\right],\quad f_2 = \frac{\Omega_{Gr}A_1 + \Omega_{MgO}A_2 + \Omega_{Cu}A_3}{\Omega_{Gr} + \Omega_{MgO} + \Omega_{Cu}}, \\ f_3 = \left(1 - \Omega_{Gr} - \Omega_{MgO} - \Omega_{Cu}\right) + \left[\frac{\Omega_{Gr}(\rho\beta)_{Gr} + \Omega_{MgO}(\rho\beta)_{MgO} + \Omega_{Cu}(\rho\beta)_{Cu}}{(\rho\beta)_{Eo}}\right], \\ f_4 = \left(1 - \Omega_{Gr} - \Omega_{MgO} - \Omega_{Cu}\right) + \left[\frac{\Omega_{Gr}(\rho C_\rho)_{Gr} + \Omega_{MgO}(\rho C_\rho)_{MgO} + \Omega_{Cu}(\rho C_\rho)_{Cu}}{(\rho C_\rho)_{Eo}}\right],\quad f_5 = \frac{\Omega_{Gr}A_4 + \Omega_{MgO}A_4 + \Omega_{Cu}A_4}{\Omega_{Gr} + \Omega_{MgO} + \Omega_{Cu}}, \end{gathered} \tag{11b}$$

Note: For simplicity, the sign * has been removed. Using the assumed solution to solve the dust particle momentum equation:

$$\Psi_1 = \Psi_{10}(y)e^{i\omega t}. \tag{12}$$

After some calculation, we get:

$$\Psi_1(\zeta,t)=\frac{l_2}{(mi\omega+l_1)}\Psi(\zeta,t). \tag{13}$$

5. Discretization of the Fractal-Fractional Model

Substituting Eq. (13) into Eq. (8), and then transforming Eqs. (8) and (9) into a fractal-fractional framework by applying Eq. (10), yields (omitting the * symbol for conciseness) [58-59]:

$$f_1\left[{}^{FF}D_\tau^{\alpha,\beta}\{\Psi(y,\tau)\}\right]=\left[f_2\frac{\partial^2\Psi(y,\tau)}{\partial y^2}-f_1\beta_2\Psi(y,\tau)-H.\Psi(y,\tau)+(f_3Gr_\tau)\theta(y,\tau)\cos(a)\right], \tag{14}$$

where, $K\left(1-\frac{l_2}{(mi\omega+l_1)}\right)=H$, and,

$$\Pr{}^{FF}D_\tau^{\alpha,\beta}(\theta(y,\tau))=\left(\frac{f_5+Nr}{f_4}\right)\frac{\partial^2\theta(y,\tau)}{\partial y^2}. \tag{15}$$

Here, ${}^{FF}D_\tau^{\alpha,\beta}\psi$ is the fractal-fractional operator of the exponential kernel [60]:

$${}^{FF}D_\tau^{\alpha,\beta}U(\tau)=\frac{N(\alpha)}{1-\alpha}\frac{d}{d\tau^\beta}\int_0^\tau U(y)\exp\left\{-\frac{\alpha}{1-\alpha}(\tau-y)\right\}dy \quad 0<\alpha,\beta\le 1. \tag{16}$$

where, $N(0)=N(1)=1$. For some positive integer N, the grid size in time for the finite difference technique is defined by [60]:

$$\lambda=\frac{1}{N}. \tag{17}$$

The grid points in the time interval [0, T] are labeled by $\tau_n=n\lambda$, with $0\le n\le N$. The value of the function at the grid point is $U_i^j=U(y_i,\tau_j)$. A numerical approximation of the fractal-fractional operator can be derived using a straightforward quadrature scheme as outlined below:

$${}^{FF}D_\tau^{\alpha,\beta}U(\tau_i)=\frac{N(\alpha)}{1-\alpha}\frac{d}{d\tau_i^\beta}\int_0^{\tau_i}U(y)\exp\left\{-\frac{\alpha}{1-\alpha}(\tau_i-y)\right\}dy \quad 0<\alpha,\beta\le 1. \tag{18}$$

$$\Rightarrow {}^{FF}D_\tau^{\alpha,\beta}U(\tau_i)=\frac{N(\alpha)}{1-\alpha}\beta\tau^{\beta-1}\sum_{j=1}^{m}\int_{(j-1)k}^{jk}\left(\frac{U_i^{k+1}-U_i^k}{\lambda}+O(\lambda)\right)\exp\left\{-\frac{\alpha}{1-\alpha}(\tau_i-y)\right\}dy, \tag{19}$$

which is equivalent to:

$${}^{FF}D_\tau^{\alpha,\beta}U(\tau_i)=\frac{N(\alpha)}{1-\alpha}\beta\tau^{\beta-1}\sum_{j=1}^{m}\left(\frac{U_i^{k+1}-U_i^k}{\lambda}+O(\lambda)\right)\int_{(j-1)k}^{jk}\exp\left\{-\frac{\alpha}{1-\alpha}(\tau_i-y)\right\}dy. \tag{20}$$

Final discretization:

$${}^{FF}D_\tau^{\alpha}U(y,\tau)=\frac{N(\alpha)}{\alpha}\beta\tau^{\beta-1}\left(\frac{U_i^{j+1}-U_i^j}{\lambda}+\sum_{j=1}^{m}\left(\frac{U_i^{j+1-m}-U_i^{j-m}}{\lambda}+O(\lambda)\right)\right)\delta_{j,m}. \tag{21}$$

Here, $\delta_{j,m}=erf\left(\frac{\alpha j}{1-\alpha}(m-j)\right)-erf\left(\frac{\alpha j}{1-\alpha}(m-j+1)\right)$. In a similar manner, using the approach outlined in [61], the first and second-order classical derivatives can be approximated in discrete form as follows:

$$\frac{\partial U(y,\tau)}{\partial y}=\frac{1}{2}\left(\frac{U_{i+1}^{j+1}-U_{i-1}^{j+1}}{2h}+\frac{U_{i+1}^{j}-U_{i-1}^{j}}{2h}\right), \tag{22}$$

$$\frac{\partial^2 U(y,\tau)}{\partial y^2}=\frac{1}{2}\left(\frac{\left(U_{i+1}^{j+1}-2U_i^{j+1}+U_{i-1}^{j+1}\right)+\left(U_{i+1}^{j}-2U_i^{j}+U_{i-1}^{j}\right)}{2h^2}\right)+O(\tau), \tag{23}$$

Using discretization Eqs. (21) to (23), Eqs. (14) and (15) become:

$$f_1\left[\frac{N(\alpha)}{\alpha}\left\{\frac{\Psi_i^{j+1}-\Psi_i^j}{\lambda}+\sum_{j=1}^{m}\left(\frac{\Psi_i^{j+1-m}-\Psi_i^{j-m}}{\lambda}\right)\right\}\delta_{j,m}\right]=\beta\tau^{\beta-1}\left[f_2\left(\frac{\left(\Psi_{i+1}^{j+1}-2\Psi_i^{j+1}+\Psi_{i-1}^{j+1}\right)+\left(\Psi_{i+1}^{j}-2\Psi_i^{j}+\Psi_{i-1}^{j}\right)}{2h^2}\right)-\frac{(f_1\beta_2+H)}{2}\left(\Psi_i^{j+1}-\Psi_i^j\right)+\left(f_3Gr_\tau\cos(a)\right)\left(\theta_i^{j+1}-\theta_i^j\right)\right], \tag{24}$$

$$\Pr\left[\frac{N(\alpha)}{\alpha}\left\{\frac{\theta_i^{j+1}-\theta_i^j}{\lambda}+\sum_{j=1}^{m}\left(\frac{\theta_i^{j+1-m}-\theta_i^{j-m}}{\lambda}\right)\right\}\delta_{j,m}\right]=\beta\tau^{\beta-1}\left(\frac{f_5+Nr}{f_4}\right)\left\{\frac{\left(\theta_{i+1}^{j+1}-2\theta_i^{j+1}+\theta_{i-1}^{j+1}\right)}{2h^2}+\frac{\left(\theta_{i+1}^{j}-2\theta_i^{j}+\theta_{i-1}^{j}\right)}{2h^2}\right\}. \tag{25}$$

Consider that $y_i=ih, 0\le i\le M$ with $Mh=1$, and $\tau_n=n, 0\le n\le N$.

Table 6. Statistical investigation of % improvement in *Nu* for Ω modification.

ξ	λ	Nr	$\Omega_{Gr}=\Omega_{MgO}=\Omega_{Cu}$	Ω	Nu	% improvement
0.5	0.7	10	0.0000	0.000	0.7914	--
0.5	0.7	10	0.002	0.009	0.8123	2.21
0.5	0.7	10	0.004	0.018	0.8354	4.32
0.5	0.7	10	0.009	0.027	0.8526	7.32
0.5	0.7	10	0.014	0.036	0.8978	9.98

Table 7. Statistical investigation of *Cf* for modification of accompanying parameters.

K	Gr_T	Nr	τ	β_2	Cf
0.5	5	2	1	0.2	1.2356
0.6					1.3518
0.7					1.4952
	10				1.1994
	15				1.1485
		4			1.4912
		6			1.6854
			2		1.5914
			3		1.8791
				0.4	1.9254
				0.6	2.4517

Table 8. Computational values utilized for this study [49-51].

Features	Nanoparticle			Host fluid
	MgO	*Gr*	*Cu*	*Eo*
C_P	955	790	385	2048
β	1.8×10^{-5}	0.0000008	1.65×10^{-5}	70×10^{-5}
κ	45	5000	401	0.1404
ρ	3560	2200	8933	863

Table 9. Grid Independence test for the Nusselt number at the wall (y = 0) at time *t* = 1.0.

Spatial Grid Size (N)	Nusselt Number (Nu)	Percentage Difference (%)
20	1.9512	--
40	2.1045	7.85%
80	2.1987	4.48%
160	2.2411	1.93%
320	**2.2598**	**0.83%**
400	2.2615	0.08%

5.1. Skin friction coefficient and Nusselt number

The skin friction coefficient and Nusselt number are crucial mathematical expressions that reveal the fundamental physical properties of the flow problem. These expressions offer valuable insights into:

- Shear stress enhancement or reduction
- Thermal conductivity evaluation
- Momentum and thermal boundary layer control
- Fluid cooling performance

To investigate these phenomena, the skin friction coefficient and Nusselt number can be examined using the following relationships:

$$Cf=\left(\frac{d}{\mu_{Eo}}\right)\frac{\tau_w}{\Psi_0},\quad Nu=\frac{dq}{\kappa_{Eo}\left(T_w-T_0\right)}, \tag{26}$$

where (τ_w) and (q) represent the viscous drag and thermal flux expressions:

$$\tau_w=\mu_{thnf}\left.\frac{\partial\Psi(y,\tau)}{\partial y}\right|_{y=0},q=-\kappa_{thnf}\left.\frac{\partial T(y,\tau)}{\partial y}\right|_{y=0}. \tag{27}$$

After substituting Eq. (26) into Eq. (27), we obtain the final relationships as:

$$Cf=f_5\left.\frac{\partial\Psi(y,\tau)}{\partial y}\right|_{y=0},\quad Nu=-f_2\left.\frac{\partial T(y,\tau)}{\partial y}\right|_{y=0} \tag{28}$$

Table 10. Validation of dimensionless velocity profile.

y	Asifa et al. [50]	Present study	Absolute error
0	0	0	0
0.1	0.1002	0.0999	0.0003
0.2	0.2004	0.2	0.0004
0.3	0.3005	0.3001	0.0004
0.4	0.4006	0.4002	0.0004
0.5	0.5004	0.5001	0.0003
0.6	0.6003	0.6001	0.0002
0.7	0.7002	0.7	0.0002
0.8	0.8001	0.7999	0.0002
0.9	0.9	0.8999	0.0001
1	1	1	0

Table 11. Validation of dimensionless temperature profile.

y	Asifa et al. [50]	Present study	Absolute error
0	0	0	0
0.1	0.0987	0.099	0.0003
0.2	0.1985	0.1988	0.0003
0.3	0.2979	0.2982	0.0003
0.4	0.3969	0.3972	0.0003
0.5	0.4956	0.4959	0.0003
0.6	0.594	0.5942	0.0002
0.7	0.6921	0.6923	0.0002
0.8	0.79	0.7902	0.0002
0.9	0.8959	0.896	0.0001
1	1	1	0

Table 6 shows the improvement in the rate of heat transfer for engine oil when tripartite hybrid nanoparticles are added. It can be observed that the thermal performance is improved by 9.98% at the maximum range. This is an ideal nanofluid for scenarios that require effective dissipation of heat.

Table 7 also presents numerical results for the skin friction coefficient (Cf) under various conditions, including different Gr_T, Nr, τ, and β_2 values. The data reveals that a small radiative flux reduces skin friction, while strong natural convection and Brinkman parameter have opposing effects. These findings are crucial for managing skin friction in physical operations, where high skin friction can lead to increased pumping power requirements. Table 8 provides a comprehensive list of computational values used in this study, serving as a valuable resource for future research and reference.

Table 9 presents the grid size increases from N = 20 to N = 400, the calculated Nusselt number converges to a stable value. The significant change observed with coarse grids diminishes rapidly. The percentage difference between the results for N = 320 and N = 400 is merely **0.08%**, which is well below our convergence threshold. Therefore, a spatial grid size of **N = 320** nodes is selected for all simulations presented in this study. This ensures that the results for velocity, temperature, skin friction, and Nusselt number are grid-independent, and any further mesh refinement would not meaningfully alter the conclusions of this work.

Table 10 presents the validation of the dimensionless velocity profile by comparing the results of the present study with those reported by Asifa et al. [50]. It is evident that the two sets of results are in very close agreement over the entire channel domain $0 \le y \le 1$. The absolute error remains extremely small, ranging from **0.0000** to **0.0004**, which confirms the accuracy and consistency of the present formulation. In particular, the velocity values at the boundaries and intermediate positions almost coincide with the benchmark data, indicating that the proposed mathematical model and the adopted computational procedure are reliable. This close agreement verifies that the present method accurately captures the momentum transport characteristics of the flow field and can therefore be used with confidence for the subsequent parametric analysis.

Table 11 shows the validation of the dimensionless temperature profile through comparison with the results of Asifa et al. [50]. The comparison demonstrates excellent agreement throughout the computational domain, with absolute errors lying between **0.0000** and **0.0003** only. Such small deviations indicate that the present thermal model correctly reproduces the heat transfer behavior reported in the reference study. The agreement at both the wall region and the interior points of the channel confirms the stability and correctness of the adopted solution procedure. Hence, the results listed in Table 11 provide strong evidence that the present study accurately predicts the thermal field and that the proposed model is suitable for examining the influence of different physical parameters on temperature distribution.

6. Results and Analysis

This study investigates the thermal behavior of a tripartite hybrid nanofluid flowing through a channel geometry. The nanofluid consists of graphene, magnesium oxide, and copper nanoparticles dispersed in engine oil. A fractal-fractional model incorporating a power law kernel is established. The model takes into account different shapes of nanoparticles. A uniform plate velocity and temperature difference cause fluid motion and heat transfer. The work focuses on the study of thermo-physical properties and energy and flow distribution in terms of different shapes of nanoparticles. Graphical solutions are provided to demonstrate different shapes of flow and influences of energy distribution resulting from radiative flux and parameters. The results are displayed in graphs and tables to describe Nusselt number, skin friction, and temperature fields. The results show the influence of flow and energy distribution with different shapes of nanoparticles. The models and results are compared with different shapes of nanoparticles and fractal-fractional and purely fractional models.

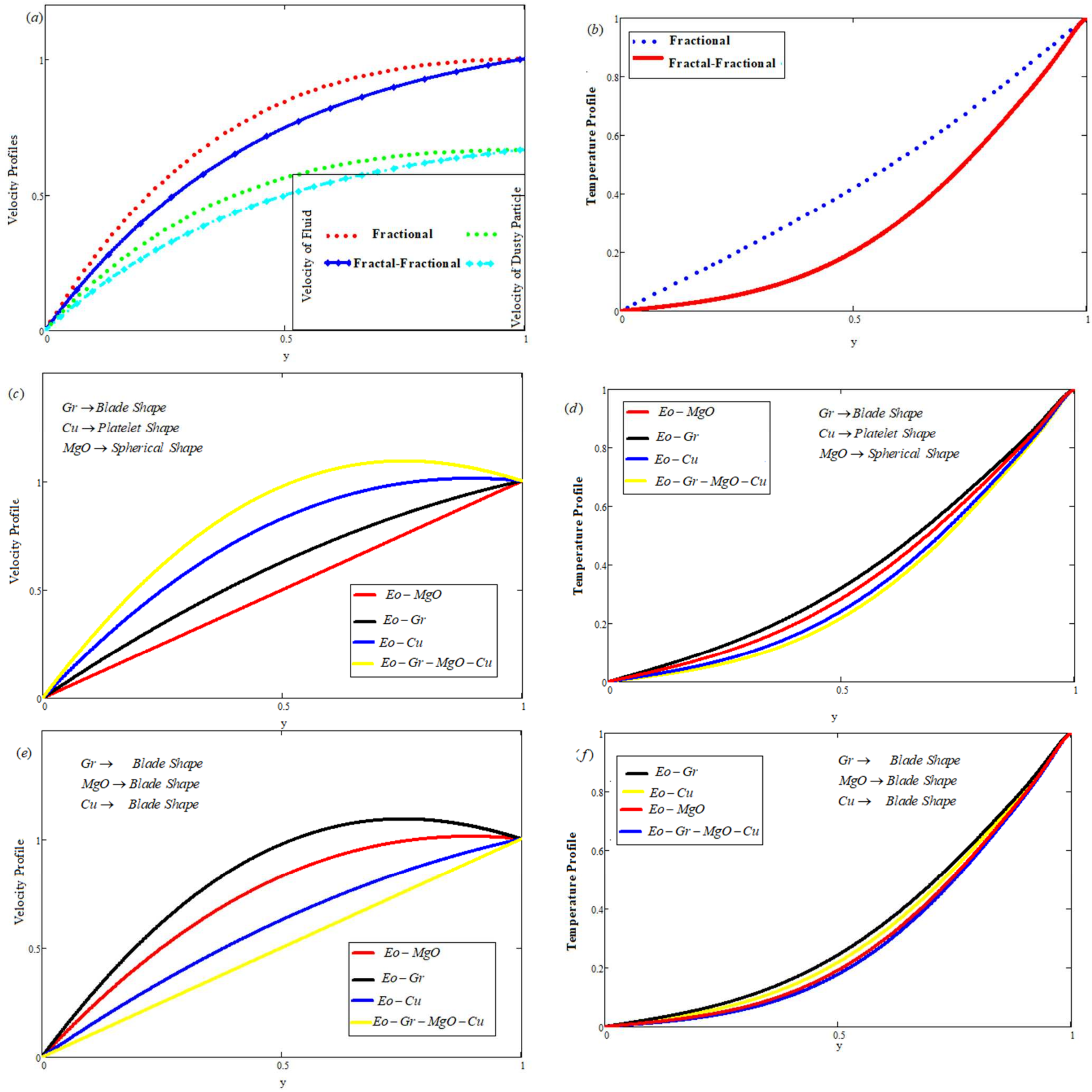

Fig. 2. Comparison between velocity and temperature profiles.

Figures 2(a) and 2(b) enable a comparison between solutions derived from the fractal-fractional method and those derived from the fractional operator method. It is manifested in the figures that the fractional approach presents more accurate solutions for velocity and temperature fields compared to the fractal-fractional method. The general operators, which are characterized by specific kernels, treat memory effects differently. It is shown within the context of this research that there is a link between the fractional and fractal operators by proposing a new parameter. The implications of variations in parameters and on the fields of energy and flow indicate improved boundary layers caused by the application of the fractal-fractional method. Figure 2(c) illustrates the comparative analysis of nanoparticles with different shapes distributed in the base fluid. The thermal curve of the resulting tripartite hybrid nanofluid (Eo-MgO-Cu-Gr) is lower than those of the individual nanofluids (Eo-MgO, Eo-Cu, and Eo-Gr). This indicates that the simultaneous suspension of three nanoparticles in engine oil increases the fluid's viscosity, making the tripartite hybrid nanofluid more viscous than the individual nanofluids. In contrast, Fig. 2(e) shows the comparative study of nanoparticles with the same shapes distributed in the base fluid. The Eo-MgO-Cu-Gr trihybrid nanoparticle exhibits the minimum velocity among all the nanoparticles, suggesting that the combination of three nanoparticles in engine oil disrupts the fluid's viscous nature, leading to a more viscous fluid. The difference in nanoparticle densities also contributes to these flow behaviors. The curves in Figs. 2(d) and 2(f) exhibit different patterns, indicating the impact of nanoparticle shape on the fluid's thermal behavior. Figure 2(d) presents the thermal field graph when nanoparticles Gr, MgO, and Cu have blade, platelet, and spherical shapes, respectively. The highest energy curve is associated with the Eo-Gr nanofluid, attributed to the comparatively highest thermal conductivity of Gr nanoparticles. Similarly, Fig. 2(f) displays the energy profile for a uniform shape of these nanoparticles (blade shape), and the Eo-Gr nanofluid exhibits the highest energy curve. In both graphs, the trihybrid nanoparticle (Eo-MgO-Cu-Gr) exhibits the minimum temperature profile compared to the individual nanoparticles, regardless of their shapes.

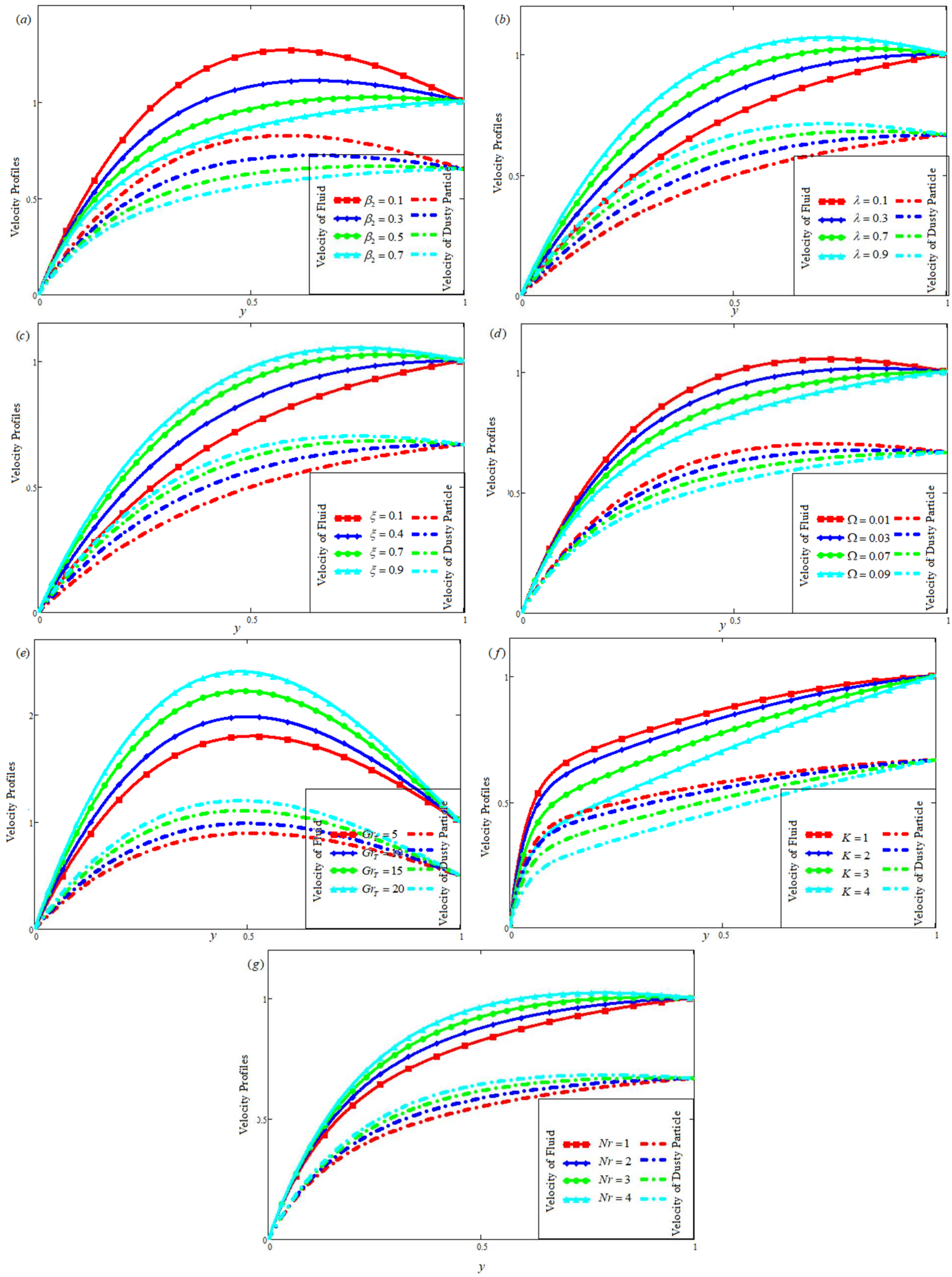

Fig. 3. The behavior of the velocity profiles for different parameters.

This suggests that the combination of three nanoparticles in engine oil leads to a more efficient heat transfer and reduced temperature profile. Overall, the study highlights the impact of nanoparticle shape and combination on the thermal behavior of nanofluids, providing valuable insights into the design and application of these advanced fluids. Figure 3(a) shows the effect of the Brinkman-fluid parameter β_2 on both the velocities (Engen oil fluid velocity and dusty fluid velocity) profile. The Brinkman-fluid parameter β_2 are increases, then both velocities profiles are presented with the reducing behavior.

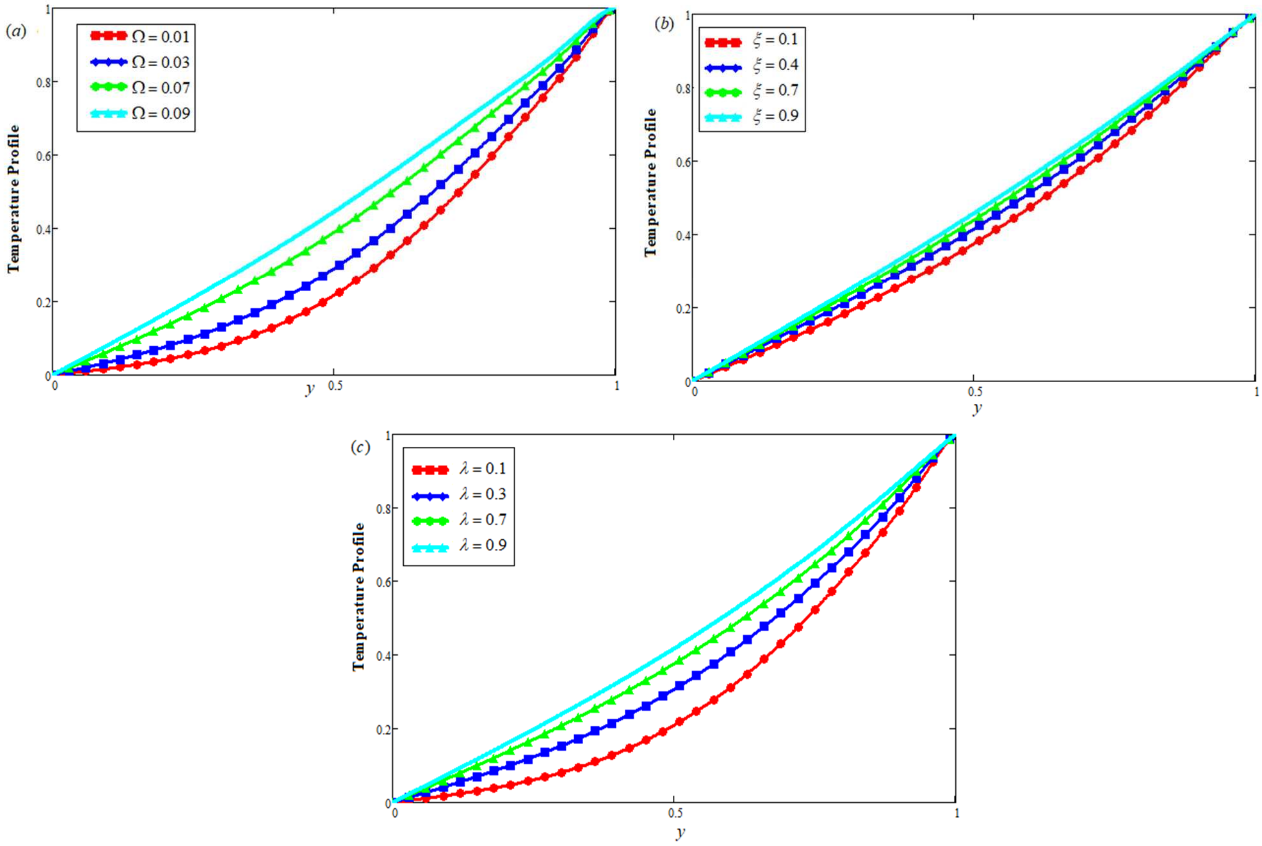

Fig. 4. The behavior of temperature profile for different parameters.

The inverse relation of the Brinkman-fluid parameter β_2 with kinematic viscosity. If the Brinkman-fluid parameter β_2 values increase, the viscosity decreases significantly, rendering its impact negligible compared to forces that support flow. This means the working fluid can overcome resistance and flow with accelerated velocity, leading to enhanced performance. In essence, the boost in β_2 values empower the fluid to dominate viscous forces, resulting in a notable improvement in flow dynamics. The dynamics of fluid flow undergo a significant transformation as the fractional (ξ) and fractal (λ) parameters are incrementally increased, as shown in Figs. 3(b) and 3(c). The flow velocity experiences a remarkable boost, showcasing the profound sensitivity of fluid behavior to these parameters. This striking visual representation highlights the potential for precision control over fluid dynamics, unlocking new possibilities for optimized performance. Figures 4(a) and 3(d) illustrate the notable findings of Colla et al. [39], who conducted a comprehensive experiment to investigate the impact of increasing nanoparticle volume concentration on the thermal conductivity and viscosity of the host fluid. Their research revealed a direct correlation between viscosity enhancement and thermal conductivity improvement, as higher nanoparticle loading ranges led to augmented property values. This study provides valuable insights into the synergistic effects of nanoparticles on fluid properties, shedding light on the potential for optimized thermal management and fluid dynamics. The Grashof number (Gr_T) emerges as a pivotal parameter in deciphering the complex dynamics of tripartite hybrid nanofluids. As Gr_T increases, the buoyancy force gains prominence, yielding a notable escalation in the flow both velocities. This phenomenon is rooted in the temperature surge at the boundary surface, inducing density gradients and diminished internal friction. Consequently, the convection current strengthens, surpassing the viscous forces and culminating in a substantial augmentation of flow speed. Both the velocities profiles in Fig. 3(e) vividly illustrate this correlation, underscoring the significance of Gr_T in predicting the flow behavior of tripartite hybrid nanofluids. Figure 3(f) shows the effect of variations in a dusty fluid parameter on the corresponding velocity profiles. Assumptions in the given problem include spherical dust particles, where the drag force is given by the Stokes drag force. From the figure, it is clear that as the value of the dusty parameter rises, the viscous force in the viscoelastic dusty fluid is reduced, resulting in the increase of velocity. A higher value of the dusty parameter results in a higher concentration of dust, thus resulting in a higher velocity for the fluid and dust mixture. Figure 3(f) further shows that due to the effect of the dusty parameter, the viscous resistance is less, resulting in a better flow, thus increasing the velocity of the mixture. Figure 3(e) shows the effect of the radiation mechanism on thermal components. There is a notable effect of the radiation mechanism on the thermal components. There is a significant effect of the radiation mechanism on the thermal components. Moreover, Fig. 3(g) shows the effect of the radiation mechanism on the flow of the tripartite hybrid nanofluid. A stronger radiation mechanism promotes the flow of the tripartite hybrid nanofluid because the generated excessive heat excites the particles, reducing the interparticle bonds; thus, the flow takes place at a faster speed. Figures 4(b) and 4(c) exhibit identical behavior in the thermal field, revealing a direct correlation between the energy and velocity functions with fractional (ξ) and fractal (λ) parameters. This phenomenon arises from the generalization of the constructed model using the fractal-fractional approach, which incorporates a power-law kernel into the system. As a result, the graphs escalate when relevant parameters are increased, demonstrating enhanced control overflow and energy fields through fractal-fractional modeling. The associated kernel effectively captures the history of functions during the process, elucidating memory features at specific time steps. This highlights the potential of fractal-fractional approaches in accurately modeling complex phenomena and capturing subtle details in flow and energy dynamics.

When discussing Figs. 3(b), 3(c), 4(b), and 4(c), explicitly state: The increase in the fractional (ξ) parameters signify a stronger memory effect, leading to enhanced velocity/temperature profiles as the system 'remembers' its previous state for longer. Conversely, the fractal (λ) parameters modulate the influence of the complex, multi-scale geometry of the suspended phases.

7. Conclusion

This study aims to understand the behavior and thermal properties of the trihybrid nanofluid Brinkman dusty fluid that flows through two plates. This will be achieved through the development of a new model based on fractal-fractional derivatives. With this new approach, the complex behavior of the nanofluid's flow and thermal properties will be comprehended and understood. Additionally, this study will investigate the preparation of a trihybrid nanofluid consisting of Gr, MgO, and Cu nanoparticles with engine oil. Various combinations of the shapes and engine oils will be considered for the investigation of the behavior of the nanofluid based on the different shapes. Additionally, the momentum equations for engine oil, velocity, and the velocity profile for the dust particles will be separately given. Solving the system of equations will be carried out using a mix of classic and fractal transform methods. This will provide series solution representations for the flow and energy equations. These representations will be graphically elucidated by MATLAB software. A numerical and graphical analysis of Nusselt number and shear stress for different nanoparticle shapes and volume fraction is also conducted. The significant outcomes of this investigation are summarized as follows:

- The fractal-fractional model excels in capturing the memory effect, making it ideal for modeling complex fluid dynamics in applications like hydraulic fracturing.
- The addition of Gr, MgO, and Cu nanoparticles to engine oil enhances its heat transport performance by 9.98%, outperforming pure engine oil.
- The fractal and fractional parameters amplify the energy and flow profiles, intensifying the distributions.
- The temperature distribution graph peaks for the Eo-MgO-Cu-Gr nanofluid, surpassing the graphs of all other examined combinations.
- The Nusselt number varies directly with fractional and fractal parameters, enabling enhanced heat transfer in applications like high-performance heat exchangers.
- The thermal properties of the nanofluid exhibit the most significant improvement when the ternary nanoparticles have a blade-like shape, whereas the spherical shape of these nanoparticles leads to the least improvement.
- The tripartite hybrid nanofluid's boiling point increases due to the synergistic effects of the nanoparticles' shape factor and material properties. This leads to a more viscous fluid with enhanced heat-carrying capacity and improved thermal stability, making it a promising coolant for high-performance applications.
- Gr nanoparticles outperform Cu and MgO in enhancing engine oil's thermal properties, making them ideal for high-performance cooling systems in automotive and industrial applications.

Finally, some suggestions are added for future researchers:

- This study is extended by using other nanoparticles.
- Also, apply the magnetic field on the whole system uniformly.
- Also extended by using complex geometry. Like cones, cylindrical, etc.
- Also, the given model uses other techniques, like perturbation, HAM, etc.

Also, added the porosity term in the main equation, and energy equation added the radiation term.

Author Contributions

G. Ali and D. Khan planned the scheme, initiated the project, conducted the investigation, developed the methodology, implemented the software, and prepared the original draft; D. Khan reviewed the manuscript, edited the content, and supervised the work; Z. Ali reviewed the manuscript; G. Ali reviewed and edited the manuscript. The manuscript was written through the contribution of all authors. All authors discussed the results, reviewed, and approved the final version of the manuscript.

Acknowledgments

Not applicable.

Conflict of Interest

The authors declared no potential conflicts of interest concerning the research, authorship, and publication of this article.

Funding

Not applicable

Data Availability Statements

The datasets generated and/or analyzed during the current study are available from the corresponding author on reasonable request.

Nomenclature

Ψ	Velocity of Brinkman fluid	c_p	Specific heat
Ψ_1	Velocity of dusty fluid	Gr_T	Thermal Grashof number
T	Temperature	K	Dusty fluid parameter
Ψ_0	Characteristic velocity	Pr	Prandtl number
T_0	Ambient	Nr	Radiation parameter
T_w	Wall temperatures	$[\bullet]_{nf}$	Nanofluids
σ_0	Boltzmann constant	$[\bullet]_{hnf}$	Hybrid nanofluid

κ_0	Rosseland absorptivity	$[\bullet]_{thnf}$	Tetra hybrid nanofluid
β_1	Brinkman fluid parameter	μ	Dynamic viscosity
m	Dust particle mass	g	Gravitational acceleration
K_0	Stock's resistances coefficient	k	Thermal conductivity
θ	Dimensionless temperature of the fluid	t	Time
ρ	Fluid density	N_0	Number distance density of the dust particles
Ω	Volume fraction parameter		

References

[1] Oldham, K., Spanier, J., *The fractional calculus theory and applications of differentiation and integration to arbitrary order*, Elsevier, 1974.
[2] Caputo, M., Linear models of dissipation whose Q is almost frequency independent—II, *Geophysical Journal International*, 13(5), 1967, 529–539.
[3] Caputo, M., Fabrizio, M., A new definition of fractional derivative without singular kernel, *Progress in Fractional Differentiation & Applications*, 1(2), 2015, 73–85.
[4] Turkyilmazoglu, M., Hyperthermia therapy of cancerous tumor sitting in breast via analytical fractional model, *Computers in Biology and Medicine*, 164, 2023, 107271.
[5] Turkyilmazoglu, M., An efficient computational method for differential equations of fractional type, *CMES-Computer Modeling in Engineering & Sciences*, 133(1), 2022, 47-65.
[6] Turkyilmazoglu, M., Altanji, M., Fractional models of falling object with linear and quadratic frictional forces considering Caputo derivative, *Chaos, Solitons & Fractals*, 166, 2023, 112980.
[7] Atangana, A., Baleanu, D., New fractional derivatives with nonlocal and non-singular kernel: theory and application to heat transfer model, *arXiv preprint*, arXiv:1602.03408, 2016.
[8] Atangana, A., Koca, I., Chaos in a simple nonlinear system with Atangana–Baleanu derivatives with fractional order, *Chaos, Solitons & Fractals*, 89, 2016, 447–454.
[9] Alkahtani, B. S. T., Chua's circuit model with Atangana–Baleanu derivative with fractional order, *Chaos, Solitons & Fractals*, 89, 2016, 547–551.
[10] Khan, D., Ali, G., Khan, A., Khan, I., Chu, Y. M., Nisar, K. S., A new idea of fractal-fractional derivative with power law kernel for free convection heat transfer in a channel flow between two static upright parallel plates, *Computer Modeling in Engineering & Sciences*, 65(2), 2020, 1237–1251.
[11] Turkyilmazoglu, M., Alofi, A. S., Liquid vortex formation in a swirling container considering fractional time derivative of Caputo, *Fractal and Fractional*, 8(4), 2024, 231.
[12] Shloof, A. M., Senu, N., Ahmadian, A., Long, N. N., Salahshour, S., Solving fractal-fractional differential equations using operational matrix of derivatives via Hilfer fractal-fractional derivative sense, *Applied Numerical Mathematics*, 178, 2022, 386–403.
[13] Khan, I., Alqahtani, A. M., Khan, A., Khan, D., Ganie, A. H., Ali, G., New results of fractal fractional model of drilling nanoliquids with clay nanoparticles, *Fractals*, 30(01), 2022, 2250024.
[14] Gangadhar, K., Shashidhar Reddy, K., Wakif, A., Wall jet plasma fluid flow problem for hybrid nanofluids with Joule heating, *International Journal of Ambient Energy*, 44(1), 2023, 2459–2468.
[15] Gangadhar, K., Rani, M. S., Subbarao, K., Wakif, A., Analysis of Carreau triple nanoparticle suspension on flow over an elongating surface with ohmic dissipation, *The European Physical Journal Plus*, 138(11), 2023, 1035.
[16] Gangadhar, K., Prameela, M., Chamkha, A. J., GR, B., Kannan, T., Evaluation of homogeneous-heterogeneous chemical response on Maxwell-fluid flow through spiraling disks with nonlinear thermal radiation using numerical and regularized machine learning methods, *International Journal of Modelling and Simulation*, 46, 2026, 100-122.
[17] Khan, D and Ali, G. Comparative study of dusty tetra hybrid Casson nanofluid flowing in a generalized two-phase MHD medium between parallel microplates with a porous medium, *The European Physical Journal Special Topics*, 233, 2024, 2225-2243.
[18] Gangadhar, K., Kumari, M. A., Venkata Subba Rao, M., Chamkha, A. J., Oldroyd-B nanoliquid flow through a triple stratified medium submerged with gyrotactic bioconvection and nonlinear radiations, *Arabian Journal for Science and Engineering*, 47(7), 2022, 8863–8875.
[19] Kotha, G., Kolipaula, V. R., Venkata Subba Rao, M., Penki, S., Chamkha, A. J., Internal heat generation on bioconvection of an MHD nanofluid flow due to gyrotactic microorganisms, *The European Physical Journal Plus*, 135, 2020, 1–19.
[20] Gangadhar, K., Bhanu Lakshmi, K., El-Sapa, S., Venkata Subba Rao, M., Chamkha, A. J., Thermal energy transport of radioactive nanofluid flow submerged with microorganisms with zero mass flux condition, *Waves in Random and Complex Media*, 35, 2025, 5779-5801.
[21] Khaliq, A., Kafafy, R., Salleh, H. M., Faris, W. F., Enhancing the efficiency of polymerase chain reaction using graphene nanoflakes, *Nanotechnology*, 23(45), 2012, 455106.
[22] Sreekumar, S., Shah, N., Mondol, J., Hewitt, N., Chakrabarti, S., Broadband absorbing mono blended and hybrid nanofluids for direct absorption solar collector: A comprehensive review, *Nano Futures*, 6, 2022, 022002.
[23] Taylor, R. A., Phelan, P. E., Otanicar, T. P., Adrian, R., Prasher, R., Nanofluid optical property characterization: towards efficient direct absorption solar collectors, *Nanoscale Research Letters*, 6(1), 2011, 1–11.
[24] Tian, S., Arshad, N. I., Toghraie, D., Eftekhari, S. A., Hekmatifar, M., Using perceptron feed-forward artificial neural network (ANN) for predicting the thermal conductivity of graphene oxide-Al2O3/water-ethylene glycol hybrid nanofluid, *Case Studies in Thermal Engineering*, 26, 2021, 101055.
[25] Alkasmoul, F. S., Al-Asadi, M. T., Myers, T. G., Thompson, H. M., Wilson, M. C. T., A practical evaluation of the performance of Al2O3-water, TiO2-water and CuO-water nanofluids for convective cooling, *International Journal of Heat and Mass Transfer*, 126, 2018, 639–651.
[26] Khan, D., Kumam, P., Khan, I., Khan, A., Watthayu, W., Arif, M., Scientific investigation of a fractional model based on hybrid nanofluids with heat generation and porous medium: applications in the drilling process, *Scientific Reports*, 12(1), 2022, 1–13.
[27] Leong, K. Y., Ahmad, K. K., Ong, H. C., Ghazali, M. J., Baharum, A., Synthesis and thermal conductivity characteristic of hybrid nanofluids – a review, *Renewable and Sustainable Energy Reviews*, 75, 2017, 868–878.
[28] Khan, D., Kumam, P., Khan, I., Sitthithakerngkiet, K., Khan, A., Ali, G., Unsteady rotating MHD flow of a second-grade hybrid nanofluid in a porous medium: Laplace and Sumudu transforms, *Heat Transfer*, 51, 2022, 8065-8083.
[29] Saqib, M., Khan, I., Shafie, S., Application of fractional differential equations to heat transfer in hybrid nanofluid: modeling and solution via integral transforms, *Advances in Difference Equations*, 2019(1), 2019, 1–18.
[30] Esmaeili, Z., Akbarzadeh, S., Rashidi, S., Valipour, M. S., Effects of hybrid nanofluids and turbulator on efficiency improvement of parabolic trough solar collectors, *Engineering Analysis with Boundary Elements*, 148, 2023, 114–125.
[31] Hussain, S. M., Entropy generation and thermal performance of Williamson hybrid nanofluid flow used in solar aircraft application as the main coolant in parabolic trough solar collector, *Waves in Random and Complex Media*, 35, 2025, 9930-9963.
[32] Esfe, M. H., Eftekhari, S. A., Hekmatifar, M., Toghraie, D., A well-trained artificial neural network for predicting the rheological behavior of MWCNT–Al2O3 (30–70%)/oil SAE40 hybrid nanofluid, *Scientific Reports*, 11(1), 2021, 17696.
[33] He, J. H., Elgazery, N. S., Elagamy, K., Abd Elazem, N. Y., Efficacy of a modulated viscosity-dependent temperature/nanoparticles concentration parameter on a nonlinear radiative electromagneto-nanofluid flow along an elongated stretching sheet, *Journal of Applied and Computational Mechanics*, 9(3), 2023, 848–860.
[34] He, J. H., Abd Elazem, N. Y., The carbon nanotube-embedded boundary layer theory for energy harvesting, *Facta Universitatis, Series: Mechanical Engineering*, 20(2), 2022, 211–235.
[35] Sun, Y. L., Shah, N. A., Khan, Z. A., Mahrous, Y. M., Ahmad, B., Chung, J. D., Khan, M. N., Exact solutions for natural convection flows of generalized Brinkman type fluids: A Prabhakar-like fractional model with generalized thermal transport, *Case Studies in Thermal Engineering*, 26, 2021, 101126.

[36] Khan, D., Almusawa, M. Y., Hamali, W., Akbar, M. A., Analysis of a two-phase MHD free convection generalized water–ethylene glycol (50:50) dusty Brinkman-type nanofluid pass through microchannel, *Journal of Mathematics*, 2023(1), 2023, 3099858.
[37] Khan, D., Murtaza, S., Ali, M., Stokes problems for transient flow of Brinkman type fluid between two side walls over an infinite plate, *City University International Journal of Computational Analysis*, 4(01), 2020, 36–59.
[38] Khan, D., Ullah, S., Kumam, P., Watthayu, W., Ullah, Z., Galal, A. M., A generalized dusty Brinkman type fluid of MHD free convection two phase flow between parallel plates, *Physics Letters A*, 450, 2022, 128368.
[39] Siddiqa, S., Hossain, M. A., Saha, S. C., Two-phase natural convection flow of a dusty fluid, *International Journal of Numerical Methods for Heat & Fluid Flow*, 25(7), 2015, 1542–1556.
[40] Khan, D., Ali, G., Ghazwani, H. A., Enhancing heat transfer in MHD Falkner's-Skan flow with thermal radiation, free convection and dusty fluid between parallel plates, *Heat Transfer*, 53(3), 2024, 1408–1424.
[41] Khan, D., Kumam, P., ur Rahman, A., Ali, G., Sitthithakerngkiet, K., Watthayu, W., Galal, A. M., The outcome of Newtonian heating on Couette flow of viscoelastic dusty fluid along with the heat transfer in a rotating frame: second law analysis, *Heliyon*, 8(9), 2022, e10538.
[42] Rostami, S., Toghraie, D., Esfahani, M. A., Hekmatifar, M., Sina, N., Predict the thermal conductivity of SiO2/water–ethylene glycol (50:50) hybrid nanofluid using artificial neural network, *Journal of Thermal Analysis and Calorimetry*, 143(2), 2021, 1119–1128.
[43] Khan, D., Rahman, A., Ali, G., Kumam, P., Kaewkhao, A., Khan, I., The effect of wall shear stress on two phase fluctuating flow of dusty fluids by using Light Hill technique, *Water*, 13, 2021, 1587.
[44] Zuo, Y. T., Variational principle for a fractal lubrication problem, *Fractals*, 32(05), 2024, 1–6.
[45] Kou, S. J., He, C. H., Men, X. C., He, J. H., Fractal boundary layer and its basic properties, *Fractals*, 30(09), 2022, 2250172.
[46] Bardos, C., Golse, F., Perthame, B., The Rosseland approximation for the radiative transfer equations, *Communications on Pure and Applied Mathematics*, 40(6), 1987, 691–721.
[47] Rajagopal, K. R., Ruzicka, M., Srinivasa, A. R., On the Oberbeck-Boussinesq approximation, *Mathematical Models and Methods in Applied Sciences*, 6(08), 1996, 1157–1167.
[48] Khan, I., Khan, D., Ali, G., Khan, A., Effect of Newtonian heating on two-phase fluctuating flow of dusty fluid: Poincaré–Lighthill perturbation technique, *The European Physical Journal Plus*, 136, 2021, 1–17.
[49] Chamkha, A. J., Rashad, A. M., Alsabery, A. I., Abdelrahman, Z. M. A., Nabwey, H. A., Impact of partial slip on magneto-ferrofluids mixed convection flow in the enclosure, *Journal of Thermal Science and Engineering Applications*, 12(5), 2020, 051002.
[50] Asifa, A., Anwar, T., Kumam, P., Sitthithakerngkiet, K., Muhammad, S., A fractal–fractional model-based investigation of shape influence on thermal performance of tripartite hybrid nanofluid for channel flows, *Numerical Heat Transfer, Part A: Applications*, 85(2), 2024, 155–186.
[51] Colla, L., Fedele, L., Scattolini, M., Bobbo, S., Water-based Fe2O3 nanofluid characterization: thermal conductivity and viscosity measurements and correlation, *Advances in Mechanical Engineering*, 4, 2012, 674947.
[52] Ali, F., Aamina, B., Khan, I., Sheikh, N. A., Saqib, M., Magnetohydrodynamic flow of Brinkman-type engine oil based MoS2-nanofluid in a rotating disk with Hall effect, *International Journal of Heat and Technology*, 4(35), 2017, 893–902.
[53] Sulochana, C., Aparna, S. R., Sandeep, N., Magnetohydrodynamic MgO/CuO-water hybrid nanofluid flow driven by two distinct geometries, *Heat Transfer*, 49(6), 2020, 3663–3682.
[54] Jamshed, W., Uma Devi, S. S., Safdar, R., Redouane, F., Nisar, K. S., Eid, M. R., Comprehensive analysis on copper-iron (II, III)/oxide-engine oil Casson nanofluid flowing and thermal features in parabolic trough solar collector, *Journal of Taibah University for Science*, 15(1), 2021, 619–636.
[55] Saqib, M., Khan, I., Shafie, S., Shape effect in magnetohydrodynamic free convection flow of sodium alginate-ferrimagnetic nanofluid, *Journal of Thermal Science and Engineering Applications*, 11(4), 2019, 041019.
[56] Hamilton, R. L., Crosser, O. K., Thermal conductivity of heterogeneous two-component systems, *Industrial & Engineering Chemistry Fundamentals*, 1(3), 1962, 187–191.
[57] He, C. H., Liu, C., Fractal dimensions of a porous concrete and its effect on the concrete's strength, *Facta Universitatis, Series: Mechanical Engineering*, 21(1), 2023, 137–150.
[58] He, J. H., Periodic solution of a micro-electromechanical system, *Facta Universitatis, Series: Mechanical Engineering*, 22, 2024, 187-198.
[59] He, J. H., He, C. H., Qian, M. Y., Alsolami, A. A., Piezoelectric biosensor based on ultrasensitive MEMS system, *Sensors and Actuators A: Physical*, 376, 2024, 115664.
[60] Atangana, A., Alqahtani, R. T., Numerical approximation of the space-time Caputo-Fabrizio fractional derivative and application to groundwater pollution equation, *Advances in Difference Equations*, 2016(1), 2016, 1–13.
[61] Smith, G. D., *Numerical solution of partial differential equations: finite difference methods*, Oxford University Press, 1985.

ORCID iD

Gohar Ali http://orcid.org/0009-0008-0801-725X
Dolat Khan https://orcid.org/0000-0002-3723-0796
Zeeshan Ali https://orcid.org/0009-0002-3443-2840

How to cite this article: Ali G., Khan D., Ali Z. Modeling Complex Flow and Heat Transfer in Engine Oil Suspended with Gr/MgO/Cu Nanoparticles Using Fractal-Fractional Derivatives, *J. Appl. Comput. Mech.*, xx(x), 2026, 1–15. https://doi.org/10.22055/jacm.2026.48653.5397